Replication of Oral BK Virus in Human Salivary Gland Cells

Raquel Burger-Calderon,[a] Victoria Madden,[b] Ryan A. Hallett,[c] Aaron D. Gingerich,[a]* Volker Nickeleit,[b] Jennifer Webster-Cyriaque[a,d]

Microbiology and Immunology Department,[a] Pathology and Laboratory Medicine,[b] Department of Biochemistry and Biophysics,[c] Department of Dental Ecology, School of Dentistry,[d] The University of North Carolina at Chapel Hill, Chapel Hill, North Carolina, USA

BK polyomavirus (BKPyV) is the most common viral pathogen among allograft patients. Increasing evidence links BKPyV to the human oral compartment and to HIV-associated salivary gland disease (HIVSGD). To date, few studies have analyzed orally derived BKPyV. This study aimed to characterize BKPyV isolated from throat wash (TW) samples from HIVSGD patients. The replication potential of HIVSGD-derived clinical isolates HIVSGD-1 and HIVSGD-2, both containing the noncoding control region (NCCR) architecture OPQPQQS, were assessed and compared to urine-derived virus. The BKPyV isolates displayed significant variation in replication potential. Whole-genome alignment of the two isolates revealed three nucleotide differences that were analyzed for a potential effect on the viral life cycle. Analysis revealed a negligible difference in NCCR promoter activity despite sequence variation and emphasized the importance of functional T antigen (Tag) for efficient replication. HIVSGD-1 encoded full-length Tag, underwent productive infection in both human salivary gland cells and kidney cells, and expressed viral DNA and Tag protein. Additionally, HIVSGD-1 generated DNase-resistant particles and by far surpassed the replication potential of the kidney-derived isolate in HSG cells. HIVSGD-2 encoded a truncated form of Tag and replicated much less efficiently. Quantitation of infectious virus, via the fluorescent forming unit assay, suggested that HIVSGD BKPyV had preferential tropism for salivary gland cells over kidney cells. Similarly, the results suggested that kidney-derived virus had preferential tropism for kidney cells over salivary gland cells. Evidence of HIVSGD-derived BKPyV oral tropism and adept viral replication in human salivary gland cells corroborated the potential link between HIVSGD pathogenesis and BKPyV.

BK polyomavirus (BKPyV) was first isolated from the urine of a renal allograft recipient in 1971 and was subsequently identified as a member of the small DNA tumor virus family (1). BKPyV infection is ubiquitous, and seroconversion of up to 90% of the world's population by the age of 10 suggests that BKPyV transmission takes place during early childhood (2, 3). BKPyV primary infection is asymptomatic and persists latently in the kidney of immunocompetent individuals (4). Reactivation occurs under immune-suppressed conditions, such as those experienced by patients receiving organ transplants and patients infected with HIV (5). BKPyV reactivation among kidney transplant patients has been associated with BKPyV nephropathy (BKN), which is by far the most significant complication among renal transplant patients (6–8).

The BKPyV genome (5 kb) is divided into three major components: the early region, the late region, and the bidirectional viral promoter, also known as the noncoding control region (NCCR). The NCCR is the major determinant of *in vitro* replication (9) and is arbitrarily divided into five block sequences: O (142 bp), P (68 bp), Q (39 bp), R (63 bp), and S (63 bp). The blocks contain the origin of DNA replication and an array of transcription factor binding sites (TFBS) (10–13). The late region encodes the agnoprotein and the structural proteins VP1, VP2 and VP3 (4, 14). The early BKPyV genome region encodes the nonstructural viral proteins: large, small, and mini-T antigen. Large T antigen (Tag) is critical for the viral life cycle and drives the host cell into the S phase (4, 15–17). Viral DNA synthesis is initiated by Tag's helicase activity, which unwinds the origin of replication within the viral NCCR promoter (4) and subsequently recruits DNA synthetic machinery (5). As the major BKPyV transforming viral oncoprotein, Tag interacts with both pRb and p53, instigating deregulated cell growth. The Tag transformation potential is linked to the p53-binding domain located near the carboxy terminus of the protein

(18). Upon initiation of DNA replication, Tag induces late viral gene expression and represses early gene expression (19).

Given its historic link to renal pathogenesis, BKPyV has been considered a kidney-tropic virus. Data however suggest a connection between BKPyV and the oral compartment. Both respiratory (5) and fecal-oral (20) routes have been suggested as likely transmission pathways. BKPyV DNA has been detected in tonsillar biopsy specimens from immunocompetent children (21–23) and nasopharyngeal aspirates of immunocompromised and immunocompetent individuals (children and adults) (24). Finally, our group has suggested a potential link between BKPyV and the oral malady HIV-associated salivary gland disease (HIVSGD) (25, 26).

HIVSGD is among the most important HIV/AIDS-associated lesions (27). HIVSGD pathogenesis is not well understood, and present treatment strategies focus solely on symptom alleviation (25). HIVSGD is characterized by salivary gland enlargement and damage that incites xerostomia (28–31). HIVSGD diagnosis has been tied to an increased risk of lymphoma development in HIV-infected individuals (32). Finally, affected patients may suffer stigma as HIVSGD's outward appearance suggests HIV infection. As for HIVSGD etiology, molecular evidence has previously established an association between polyomaviruses (PyV) and salivary gland pathology. Rodent models demonstrated that PyV injection

resulted in salivary gland tumors in mice (33). *In vivo*, HIVSGD patients shed 20-fold-higher levels of BKPyV in throat wash (TW) and plasma (viremia) than HIV-positive patients without HIVSGD and HIV-negative individuals (25). Moreover, our group has demonstrated successful replication of a BKPyV laboratory strain in human salivary gland cell lines (HSG and HSY) *in vitro* (26). While contemporary advances have allowed efficient *in vitro* cultivation of archetype BKPyV in kidney cells (providing Tag in *trans* [34]), studies analyzing clinical BKPyV isolates have been limited and kidney focused and have not assessed salivary gland infection (9, 35–38). Molecular evidence demonstrates that the *in vivo* replication compartments of urine- and plasma-derived BKPyV are distinct (39, 40). Similarly, the salivary gland may provide an additional BKPyV replication compartment in HIVSGD (41).

In the present study, HIVSGD-derived BKPyV underwent successful replication in human salivary gland (HSG) cells, providing proof of concept that salivary glands of HIVSGD patients may be replication competent. We further compared the replication potential of TW-derived BKPyV clinical isolates to those of urine- and laboratory-derived BKPyV in HSG cells and in kidney cells (Vero). The replication potential of the clinical isolates HIVSGD-1 and HIVSGD-2 differed greatly despite the two isolates bearing the same NCCR architecture (OPQPQQS) and their genomes differing by only three nucleotides. The replication inefficiency of HIVSGD-2 was likely caused by the introduction of a stop codon that produced a truncated Tag mutant. Interestingly, HIVSGD-1 BKPyV encoded full-length Tag, replicated efficiently, and displayed preferential tropism for salivary gland cells over kidney cells, as suggested by quantitation of infectious virus.

MATERIALS AND METHODS

Patient information and sample collection. HIVSGD-positive individuals from The University of North Carolina at Chapel Hill (UNC) hospital dental clinic were selected for throat wash (TW) collection under institutional review board (IRB)-approved study guidelines. Urine samples from HIV-negative patients were kindly donated and collected under the supervision of V. Nickeleit at UNC Hospitals. Patient samples were centrifuged and DNase treated, and DNA was isolated via the Qiagen DNeasy kit, as described by the manufacturer.

BKPyV NCCR sequencing. The BKPyV NCCR was PCR amplified (Vent polymerase; New England BioLabs, Inc.) with primers BKPyVTU1F and BKPyVTU1R (37) from patient sample DNA, and the products were subsequently sequenced by Genewiz, Research Triangle Park, NC. NCCR amplification and sequencing was repeated a minimum of three times per patient sample. The resulting NCCR nucleotide sequence was analyzed and aligned by the Vector NTI program. Vector NTI identified the block motifs with a minimum similarity of 70% to original block sequences (10).

wg BKPyV cloning. Whole-genome (wg) BKPyVs, including the naturally occurring BamHI restriction fragment recognition sites, were PCR amplified from clinical samples with primers BKPyVWGF (VP1 Forward, 5′-GCGGGATCCAGATGAAAACCTTAGG-3′) and BKPyVWGR (VP1 Reverse, 5′-GCGGGATCCCCCATTTCTGG-3′), using the Expand Long Range dNTPack (Roche) as described by the manufacturer. Amplified wg BKPyV products were purified by the QIAquick PCR purification kit (Qiagen), as described by the manufacturer. Purified HIVSGD-2 and U1 wg BKPyV DNA was cloned via the TOPO TA cloning kit (Invitrogen) as described by the manufacturer. Purified HIVSGD-1 DNA and pUC18 vector (2.6 kb) from Stratagene were digested separately with restriction endonuclease BamHI, isolated, ligated via T4 DNA ligase (BioLabs). DH5α bacterial cells (Invitrogen) were transformed with the HIVSGD-1, HIVSGD-2, and MM ligation products. All bacterium-derived constructs

were isolated via QIAfilter plasmid Midi kit (Qiagen) after 24 h of incubation at 37°C.

Virus, transfection, and infection conditions. The clinical BKPyV strains cloned by us were HIVSGD-1, HIVSGD-2, and U1. The commercially available infectious BKPyV was VR837 (ATCC). The laboratory-derived Dunlop BKPyV clone was kindly donated by Michael J. Imperiale. The laboratory-derived MM (ATCC 45026) BKPyV clone (42) is commercially available. Interestingly, the MM BKPyV NCCR and Tag sequencing results obtained in this study were not homologous with previously published sequence (GenBank accession no. V01109).

BKPyV transfection. Cloned BKPyV was cut out of its respective backbones by overnight (37°C) incubation with BamHI endonuclease; HIVSGD-1 (pUC18), HIVGD-2 (pCR2.1), U1 (pCR2.1) and MM (ATCC 45026) (pBR322). wg BKPyV cloned into pCR2.1 was digested with endonuclease *Taq*1a for an additional 3 h at 65°C. wg BKPyV cloned into pBR322 was digested with endonuclease BsAa1 for an additional 3 h at 37°C. All digested samples were run on a 2% ethidium bromide (EtBr) agarose gel, and 5-kb bands were isolated in order to obtain wg BKPyV. wg BKPyV DNA was purified via the QIAquick gel extraction kit (Qiagen), as instructed by the manufacturer, and religated via T4 DNA ligase (BioLabs) overnight at 16°C. Episomal viral DNA was subsequently purified via phenol-chloroform. Single layers of HSG and Vero cells were passaged by trypsinization (~15 min), resuspended in 2% fetal bovine serum (FBS) and 1% penicillin–streptomycin culture medium, and subsequently seeded at ~30% confluence. Episomal BKPyV was introduced into the cells via lipid-mediated gene delivery, using *Trans*IT-LU1 (Mirus) according to the manufacturer's protocol. Medium was changed 48 h posttransfection (p.t.). Media and cells were collected at different time points for further analysis.

Infection. Equal amounts of infectious clinical and laboratory strain BKPyV (determined via fluorescent focus assay [FFA]) were used for infection of HSG and Vero cells—illustrated in part 2 of the *in vitro* model shown in Fig. 4. Supernatants of transfected HSG cells carrying infectious BKPyV were passed through 0.45-μm-pore filters and added to fresh HSG and Vero cells.

Cell culture. Human submandibular salivary gland epithelial cells (HSG cells) from adenocarcinoma (43) were obtained from B. Baum (NIH) and maintained in McCoy's 5A medium (Sigma) supplemented with 10% fetal bovine serum (FBS) (Sigma) and 1% penicillin–streptomycin (P/S) (Gibco). African green monkey kidney epithelial cells (Vero cells), were obtained from the American Type Culture Collection (ATCC), maintained in Dulbecco's minimal essential medium (DMEM) (Sigma) supplemented with 10% FBS and 1% P/S. Both cell lines were incubated in humidified atmosphere at 37°C and 5% CO_2.

Reporter construct formation. Primers BKPyVTU1F and BKPyVTU1R (37) were used to amplify the BKPyV NCCR with flanking SacI restriction fragment recognition sites via PCR (Vent polymerase; New England BioLabs, Inc.). Amplified DNA products were purified by QIAquick PCR purification kit (Qiagen), as described by manufacturer. Purified DNA and pGL3-Basic vector (5 kb) from Promega were digested separately with restriction endonuclease SacI, isolated, and ligated via T4 DNA ligase (BioLabs). DH5α bacterial cells (Invitrogen) were transformed with products, and constructs were isolated via the QIAfilter plasmid Midi kit (Qiagen) after 24 h of incubation at 37°C.

BKPyV NCCR promoter activity. HIVSGD-1 and HIVSGD-2 BKPyV NCCR promoter activities were measured with and without the presence of wild-type large Tag in HSG cells via the luciferase (Luc) reporter assay (pGL3 vectors; Promega). Cloned reporter constructs (1 μg) were transfected into HSG cells via lipid-mediated gene delivery, using *Trans*IT-LU1 (Mirus) according to the manufacturer's protocol. pCDNA RFP (red fluorescent protein) was cotransfected along with or without Tag (0.5 μg) expression plasmid (in pCMV myc; kindly provided by L. Jeffers). The Tag expression plasmid encoded VR837 BKPyV-derived full-length wild-type large Tag. Cells were collected from each treatment at 48 h according to the Promega luciferase assay protocol. Luc activities of the HIVSGD

TABLE 1 Demographics and viral characterization of clinical BKPyV isolates[a]

Virus strain	HIV status	Clinical status or origin	Source	Age (yr)[b]	BKPyV VL (copies/ml)	NCCR
Patient derived						
HIVSGD-1	+	HIVSGD	TW	47	1.76×10^5	OPQPQQS
HIVSGD-2	+	HIVSGD	TW	60	2.57×10^5	OPQPQQS
U1	−	BKN, lung transplant	Urine	31	1.79×10^9	OPQ
Laboratory derived						
Dunlop		Laboratory-derived clone				OPPPS
VR837		ATCC, infectious virus				OPQPQS
MM		ATCC, clone				OPQPQQS

[a] Clinical whole-genome BKPyV was cloned from two HIV-associated salivary gland disease (HIVSGD) throat wash (TW) samples (HIVSGD-1 and HIVSGD-2) and one transplant patient urine sample (U1) for *in vitro* analysis. All patients from whom the patient-derived strains were obtained were male. Laboratory strains Dunlop, VR837, and MM served as laboratory control strains. NCCR, noncoding control region; BKN, BKPyV nephropathy.
[b] Patient age at time point of sample collection.

clones, pGL3 control vector (positive control [not shown]), and pGL3-Basic vector (negative control) were measured in a microplate format by the LMAX luminometer (Molecular Devices). HIVSGD Luc activity was normalized to pGL3-Basic.

FFA. Vero cells (50% confluence) were infected with various volumes of filtered (0.45-μm pore) supernatant from transfected HSG cells and incubated over 4 days. Where low levels of virus were present, higher volumes were utilized in order to attain infection. These differences in volumes used for Vero cell infection are accounted for in calculations of fluorescence-forming units (FFU)/μl (44). Vero cells were fixed in 50:50 methanol-acetone, air dried, and stored at −80°C overnight 4 days postinfection (p.i.). Cells were rehydrated with phosphate-buffered saline (PBS) the next day and incubated with anti-JC/BK polyomavirus primary antibody NCL JCBK (Novocastra, Leica) at a 1:10 dilution in PBS for 30 min at 37°C and 30 min at room temperature (RT). The secondary antibody, goat anti-mouse-Alexa Fluor 488 (Life Technologies) conjugate at a 1:100 dilution in PBS, was added for 1 h at RT after the cells had been washed twice with PBS. Cells were washed with PBS prior to addition of DAPI (4′,6-diamidino-2-phenylindole)-DNA stain (1:10,000) and fluorescence microscopy analysis (Olympus IX81). BKPyV-infected cells were counted at a ×20 magnification for a minimum of 10 fields per dish, and FFU were calculated as described in reference 44. FFU values were graphed for each treatment and are depicted as FFU/μl or FFU/μl + 1 in order to transform the zero values for the $\log_{10}$-based *y* axis.

BKPyV DNA detection via Southern blot hybridization. BKPyV episomes were transfected (see above for BKPyV DNA and transfection details) into HSG cells at the following concentrations: 0.39 μg Dunlop, 0.45 μg U1, 0.72 μg HIVSGD-1, 0.9 μg MM, and 0.9 μg pcDNA3 DNA. Differential amounts of DNA were transfected for the DpnI resistance assay. Hence, this assay was not intended to compare BKPyV replication levels. All succeeding experiments were intended to evaluate relative viral replication levels, and transfections were done with equal amounts of BKPyV DNA. Low-molecular-weight DNA was isolated from HSG cells 6 days p.t. by a previously described modified Hirt method (45), digested by endonucleases Sau3a and DpnI, electrophoresed on a 7% agarose gel, and transferred onto a SuPerCharge (SPC) membrane by the Whatman Nytran SPC Turbo blotter (General Electric), as described by the manufacturer. Membrane-associated BKPyV DNA was detected by hybridization to randomly primed wg MM BKPyV (ATCC 45026) ^{32}P-labeled DNA probe and exposed to film (Kodak). The expected MM BKPyV DNA band sizes according to mapped DpnI/Sau3a cut sites were 1,522, 681, 529, 451, 432, 346, 294, 230, 216, 129, and 116 bp.

Encapsidated viral DNA isolation and qPCR amplification. Transfected and infected HSG and Vero cell supernatants were passed through 0.45-μm-pore filters and DNase treated (Promega), removing debris/cells and nonencapsulated viral DNA, respectively. DNA was isolated using the QIAamp DNA blood minikit (Qiagen) as instructed by the manufacturer. Viral load (VL) was quantified via quantitative real-time PCR (qPCR)

analysis with Roche LightCycler 480 SYBR green I master mix as a detector in the Roche Light Cycler 480 by using previously published primers for VP1 (46). BKPyV plasmid, kindly donated by V. Nickeleit, was used to establish a standard curve and for subsequent quantification of encapsidated viral genomes present in the cellular supernatant.

TEM. Three milliliters of transfected, infected, or control HSG and Vero cell supernatant was spun at 13,000 rpm for 30 min at 4°C in order to remove cellular debris and then at 290,000 rpm for 1 h at 4°C by ultracentrifugation in order to concentrate BKPyV and decrease the suspension volume. Metal grids were subjected to purified supernatant and treated with 2% uralic acetate for negative staining. Virus was subsequently visualized via EM910 transmission electron microscopy (TEM) (Zeiss) utilizing a Gatan SC1000 camera.

Immunoblotting. Episomal BKPyV DNA (0.3 μg) was transfected into HSG cells, and whole-cell lysates were harvested with 1% SDS lysis buffer 4 days posttransfection. Protein was quantified using the Bio-Rad protein assay, and equal amounts were electrophoresed on a 10% Bis-Tris polyacrylamide minigel (Invitrogen). Tag antibody PAb416 (Genetex) (1:200) in 5% nonfat dry milk in 0.1% Tween 20–PBS (PBS-T) was used to detect Tag expression post-wg BKPyV transfection of HSG cells. c-Myc-tagged Tag expression was detected via anti c-Myc antibody (Santa Cruz) (1:1,000) post-reporter construct transfection of HSG cells. Actin expression was detected via the (C-11)-R sc-1615-R antibody (Santa Cruz Biotechnology) (1:1,000) in 5% nonfat dry milk (as described above). Blots were washed in PBS-T three times for 10 min at RT and probed with a horseradish peroxidase-conjugated secondary antibody (Promega) (1:10,000), exposed to SuperSignal West Pico chemiluminescent substrate (Thermo Scientific), and exposed to film (Kodak). Band intensity was measured via densitometry. Relative band density was determined by normalizing Tag to actin expression via Gene Tools from Syngene.

Nucleotide sequence accession numbers. The MM BKPyV NCCR and Tag sequencing results obtained in this study have been submitted to the GenBank database under accession no. KF445133 (BankIt1648707) and KF445132 (BankIt1648650), respectively.

RESULTS

HIVSGD-1 and HIVSGD-2 BKPyV isolation and sequence analysis. Throat wash (TW) samples were collected from two HIV-positive subjects with diagnosed HIVSGD. To obtain kidney-derived BKPyV, urine was collected from an HIV-negative lung transplant patient with diagnosed BKPyV nephropathy (BKN). Patient demographic data (HIV status, other clinical status, age, and sex) were collected, and BKPyV viral load (VL) was determined. Whole-genome (wg) BKPyVs were cloned from each sample, and the viral NCCR promoters were sequenced (Table 1). All three clinical samples had high VLs ranging from 1.7×10^5 to 1.7×10^9 copies/ml. Similar to the laboratory strain MM, both of
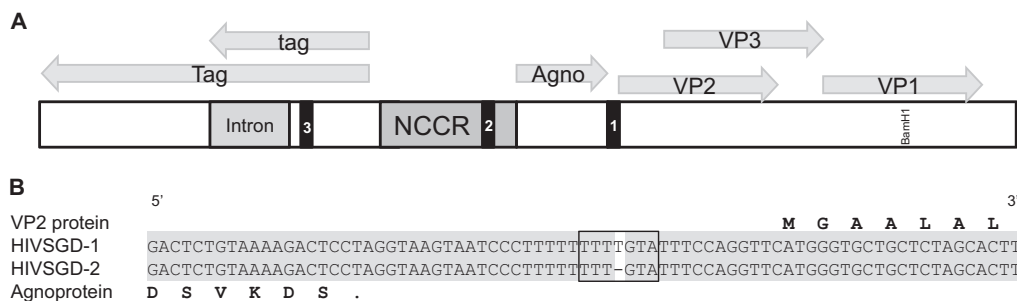
FIG 1 Whole-genome sequence comparison between HIVSGD BKPyV isolates revealed three polymorphisms. (A) The schematic shows the linearized BKPyV genome and encoded viral proteins. Black bars and numbers denote the three single-base-pair polymorphisms (black bars 1 to 3) differentiating whole genomes HIVSGD-1 and HIVSGD-2: 1, thymidine deletion between the open reading frames (ORFs) coding for agnoprotein and VP2; 2, thymidine-to-cytidine transition within the noncoding control region (NCCR); 3, adenosine deletion within the ORF coding for Tag. (B) The depicted DNA stretches show the thymidine deletion between the ORFs coding for agnoprotein and VP2 found within HIVSGD-2 but not HIVSGD-1.

the HIVSGD-derived BKPyV isolates had OPQPQQS NCCR block alignments. The transplant urine sample carried BKPyV with a OPQ NCCR block alignment. The NCCR architectures of previously studied laboratory strains MM, Dunlop, and VR837 BKPyV were sequenced as a control measure and recovered correctly (Table 1). Alignment of the whole-genome nucleotide sequences of HIVSGD-1 and HIVSGD-2 BKPyV detected 99.9% whole-genome similarity. The three single-nucleotide differences were as follows: (i) a single-base-pair thymidine (T) deletion between sequences that encoded agnoprotein and VP2 (Fig. 1A, 1), (ii) a thymidine/cytidine transition (T/C) within the NCCR (Fig. 1A, 2), and (iii) a single-base-pair adenosine (A) deletion within the Tag coding sequence (Fig. 1A, 3). All three mutations were analyzed for potential biological significance. The T deletion located between the genes coding for agnoprotein and VP2 was assumed to be least important, since this mutation did not affect either of the adjacent VP2 and agnoprotein open reading frames (Fig. 1B).

The HIVSGD-1 and HIVSGD-2 NCCRs differed by a T/C transition located within the S block of the viral promoter. To assess the potential biological significance of this nucleotide transition, putative human transcription factor binding sites (TFBS) were predicted within this region of the NCCR. Identical TFBS (Smad3, Smad4, C/EBPα, AP-2αA, and E47) were predicted for both HIVSGD-1 and HIVSGD-2 (Fig. 2A). Next, *in vitro* promoter activity was assessed to determine whether the transition led to differential promoter activity despite homologous TFBS. HIVSGD-1 and HIVSGD-2 NCCR-pGL3 reporter constructs were generated in the early and in the late directions. NCCR reporter and pGL3 basic control constructs were cotransfected with (black bars) and without (white bars) full-length VR837-derived Tag in HSG cells (Fig. 2B and C). Promoter activity was determined as fold luciferase (Luc) induction over pGL3-Basic. Tag protein expression was confirmed by immunoblot analysis. Similar promoter activity levels were achieved for both HIVSGD-1 and HIVSGD-2 in the early direction, independent of Tag's presence or absence: 2.7- versus 2.4-fold and 12- versus 11.4-fold induction, respectively (Fig. 2B). HIVSGD-2 promoter activity was higher than that of HIVSGD-1 in the late direction independent of Tag's presence or absence: 54- versus 31-fold and 7- versus 2-fold induction, respectively (Fig. 2C). Overall, NCCR activity differences between HIVSGD-1 and HIVSGD-2 were nominal. Functional Tag is known to suppress the BKPyV NCCR in the early

direction and induce it in the late direction (4). Hence, the observations made here suggested that the cloned HIVSGD NCCRs were functional within the reporter constructs.
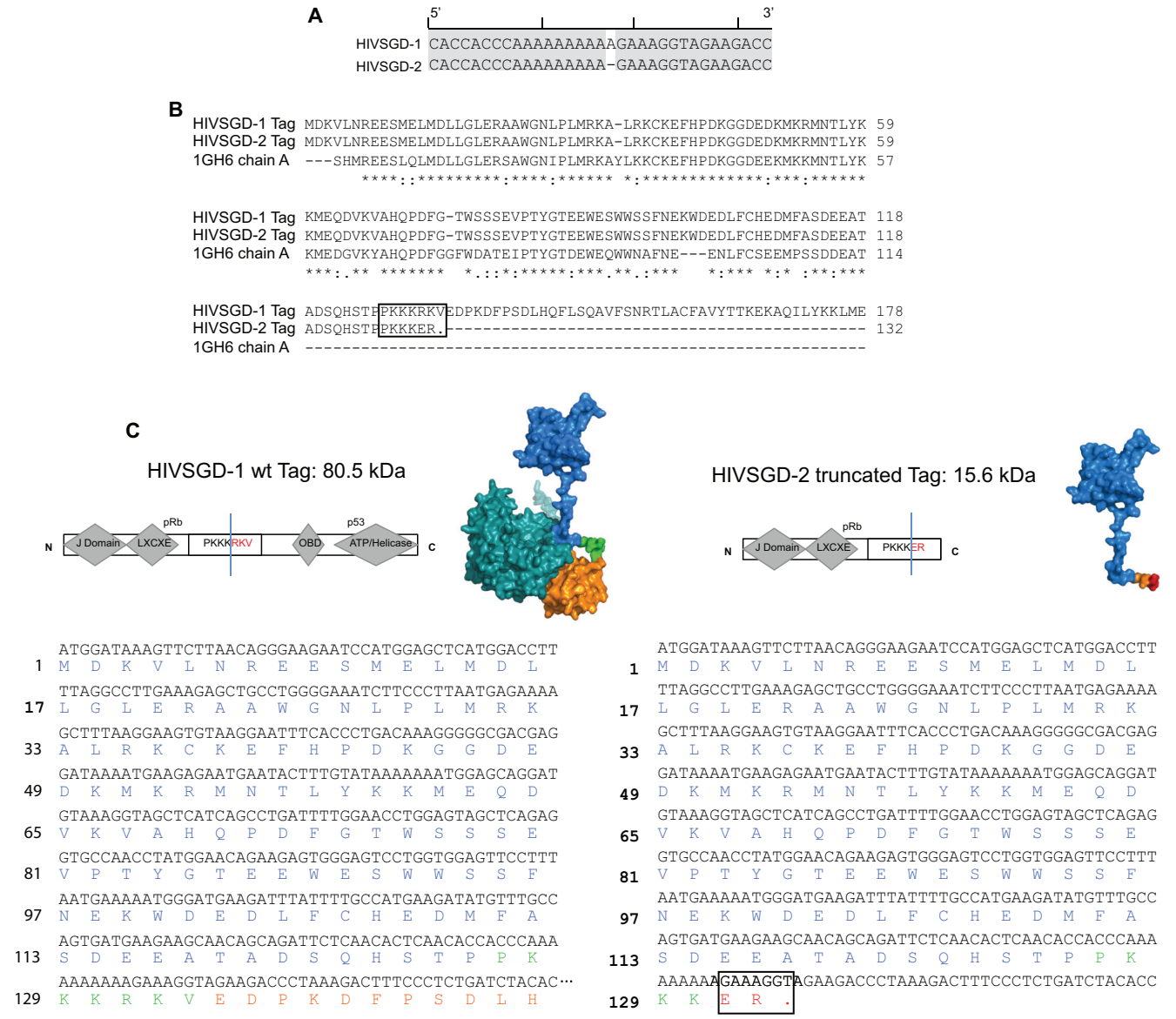
The adenosine (A) deletion detected within the Tag nucleotide sequence of HIVSGD-2 but not within HIVSGD-1 was analyzed for potential biological significance (Fig. 3A). ClustalW (47)-based Tag amino acid sequence alignment of HIVSGD-1, HIVSGD-2, and the simian virus 40 (SV40) pRb binding domain (1GH6:ChainA) located the deletion distal to the pRb binding site of the Tag viral protein and detected 82.5% sequence identity between SV40 and HIVSGD-1 full-length Tag. The deletion was predicted to introduce an early stop codon that truncated the original Tag nuclear translocation signal from PKKKRKV to PKKKER (Fig. 3B). HIVSGD-2 Tag, which carried the early stop codon, was calculated to express a Tag mutant of 15.6 kDa instead of the 80.5-kDa full-length Tag expressed by BKPyV HIVSGD-1 (Fig. 3C). A schematic model of full-length HIVSGD-1 and truncated HIVSGD-2 Tag was created using the HHPred and MODELLER structural prediction tools (48). This truncating deletion was likely the most significant of the three nucleotide mutations due to the truncation and the importance of Tag for the viral life cycle.

Assessment of HIVSGD BKPyV replication *in vitro*: posttransfection. The posttransfection replication potential of HIVSGD-1 and HIVSGD-2 BKPyV was assessed within human salivary gland and kidney cells (Fig. 4). BKPyV clones of throat wash-derived HIVSGD-1 and HIVSGD-2, kidney-derived U1, and laboratory strains MM and Dunlop were used for *in vitro* analysis (Table 1). Laboratory strain VR837 was used as an infectious BKPyV-positive control.

The capacity for *de novo* BKPyV DNA synthesis post-salivary gland cell (HSG)-transfection was determined. HSG cells were transfected with HIVSGD-1 (encoding full-length Tag), U1, MM, and Dunlop BKPyV episomes and evaluated using a restriction enzyme resistance assay. The DpnI/Sau3a enzyme resistance assay allowed discernment between transfected BKPyV genomes (methylated bacterial plasmid DNA) and BKPyV genomes made *de novo* (nonmethylated eukaryotic DNA). DNA was isolated 6 days posttransfection (p.t.), digested with DpnI and Sau3a, and visualized by Southern blotting (Fig. 5). DpnI and Sau3a cleaved the same restriction sites, but DpnI digested exclusively bacterial and not eukaryotic methylation patterns, while Sau3a digestion was methylation pattern independent (9, 49). While multiple bands were detected post-Sau3a digestion, clear differences in the
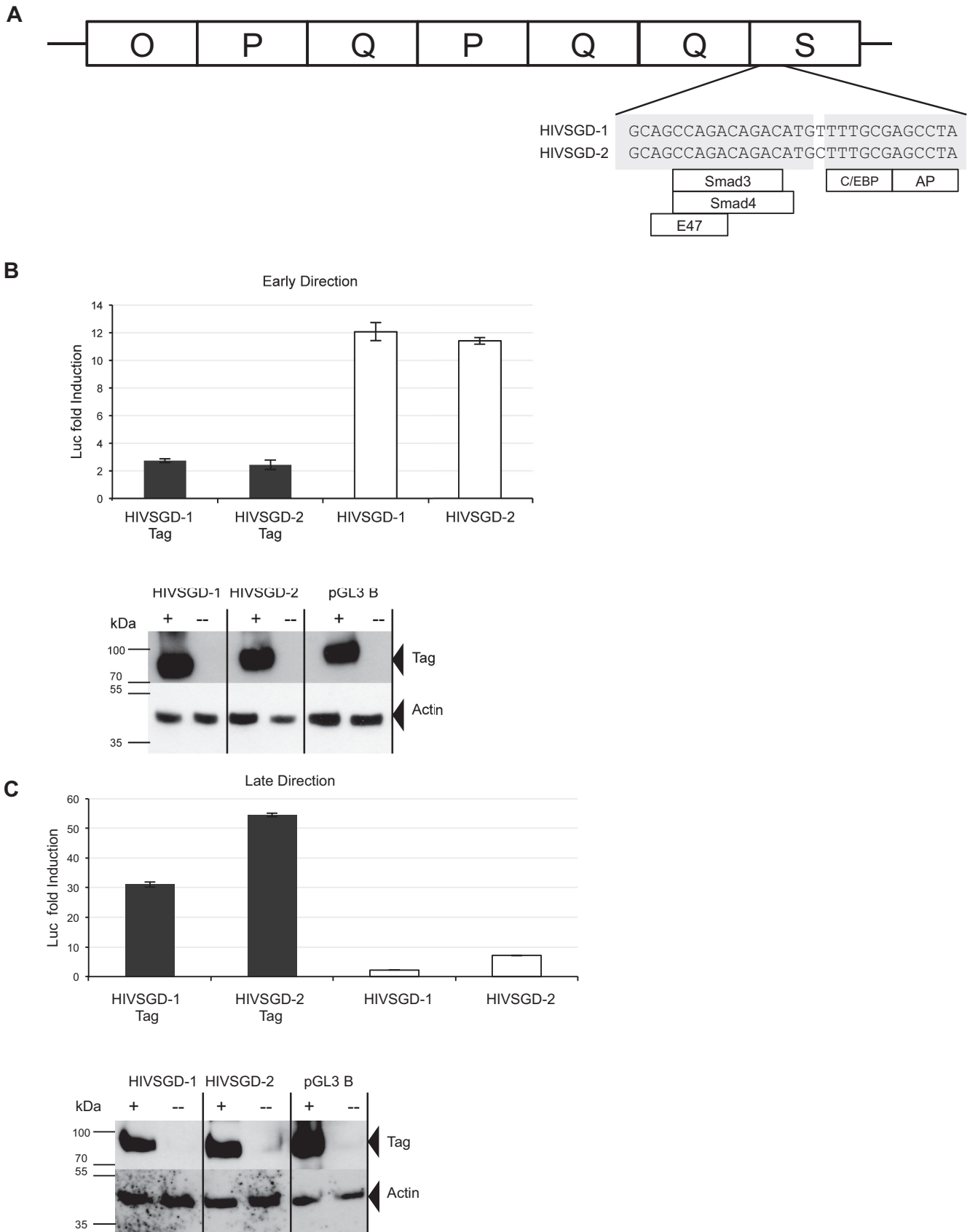
FIG 2 Similar trends in promoter activity were detected for HIVSGD-1 and HIVSGD-2 BKPyV. (A) The schematic represents the HIVSGD BKPyV NCCR block architecture and the thymidine/cytidine transition within the S block. Identical human putative transcription factor binding sites (TFBS) were predicted for HIVSGD-1 and HIVSGD-2 despite the transition: E47, Smad3, Smad4, C/EBPα (C/EBP), and AP-2αA (AP). (B and C) Graphs show NCCR luciferase (Luc) activity in the presence and absence of wild-type Tag for the early (B) and late (C) promoter directions. Luc activity was depicted as fold induction relative to pGL3-Basic (pGL3 B), and error bars represent standard deviations. Tag (Myc-tagged Tag, ~82-kDa) and actin (~45-kDa) protein expression were visualized by immunoblotting.

A

	5'			3'
HIVSGD-1	CACCACCCAAAAAAAAAAAGAAAGGTAGAAGACC			
HIVSGD-2	CACCACCCAAAAAAAAA–GAAAGGTAGAAGACC			

B

```
HIVSGD-1 Tag    MDKVLNREESMELMDLLGLERAAWGNLPLMRKA-LRKCKEFHPDKGGDEDKMKRMNTLYK   59
HIVSGD-2 Tag    MDKVLNREESMELMDLLGLERAAWGNLPLMRKA-LRKCKEFHPDKGGDEDKMKRMNTLYK   59
1GH6 chain A    ---SHMREESLQLMDLLGLERSAWGNIPLMRKAYLKKCKEFHPDKGGDEEKMKKMNTLYK   57
                   ****:.:*********:****.:****** *:*************.***:******

HIVSGD-1 Tag    KMEQDVKVAHQPDFG-TWSSSEVPTYGTEEWESWWSSFNEKWDEDLFCHEDMFASDEEAT  118
HIVSGD-2 Tag    KMEQDVKVAHQPDFG-TWSSSEVPTYGTEEWESWWSSFNEKWDEDLFCHEDMFASDEEAT  118
1GH6 chain A    KMEDGVKYAHQPDFGGFWDATEIPTYGTDEWEQWWNAFNE---ENLFCSEEMPSSDEAT  114
                ***:.** ******* *.::*:*****:***.**.:*** *:*** *:* :**:***
```

```
HIVSGD-1 Tag    ADSQHSTP PKKKRKV EDPKDFPSDLHQFLSQAVFSNRTLACFAVYTTKEKAQILYKKLME  178
HIVSGD-2 Tag    ADSQHSTP PKKKER .-------------------------------------------  132
1GH6 chain A    -----------------------------------------------------------
```

C

HIVSGD-1 wt Tag: 80.5 kDa

HIVSGD-2 truncated Tag: 15.6 kDa


```
      ATGGATAAAGTTCTTAACAGGGAAGAATCCATGGAGCTCATGGACCTT
 1    M  D  K  V  L  N  R  E  E  S  M  E  L  M  D  L
      TTAGGCCTTGAAAGAGCTGCCTGGGGAAATCTTCCCTTAATGAGAAAA
17    L  G  L  E  R  A  A  W  G  N  L  P  L  M  R  K
      GCTTTAAGGAAGTGTAAGGAATTTCACCCTGACAAAGGGGGCGACGAG
33    A  L  R  K  C  K  E  F  H  P  D  K  G  G  D  E
      GATAAAATGAAGAGAATGAATACTTTGTATAAAAAAATGGAGCAGGAT
49    D  K  M  K  R  M  N  T  L  Y  K  K  M  E  Q  D
      GTAAAGGTAGCTCATCAGCCTGATTTTGGAACCTGGAGTAGCTCAGAG
65    V  K  V  A  H  Q  P  D  F  G  T  W  S  S  S  E
      GTGCCAACCTATGGAACAGAAGAGTGGGAGTCCTGGTGGAGTTCCTTT
81    V  P  T  Y  G  T  E  E  W  E  S  W  W  S  S  F
      AATGAAAAATGGGATGAAGATTTATTTTGCCATGAAGATATGTTTGCC
97    N  E  K  W  D  E  D  L  F  C  H  E  D  M  F  A
      AGTGATGAAGAGCAACAGCAGATTCTCAACACTCAACACCACCCAAA
113   S  D  E  E  A  T  A  D  S  Q  H  S  T  P  P  K
      AAAAAAAGAAAGGTAGAAGACCCTAAAGACTTTCCCTCTGATCTACAC···
129   K  K  R  K  V  E  D  P  K  D  F  P  S  D  L  H
```

```
      ATGGATAAAGTTCTTAACAGGGAAGAATCCATGGAGCTCATGGACCTT
 1    M  D  K  V  L  N  R  E  E  S  M  E  L  M  D  L
      TTAGGCCTTGAAAGAGCTGCCTGGGGAAATCTTCCCTTAATGAGAAAA
17    L  G  L  E  R  A  A  W  G  N  L  P  L  M  R  K
      GCTTTAAGGAAGTGTAAGGAATTTCACCCTGACAAAGGGGGCGACGAG
33    A  L  R  K  C  K  E  F  H  P  D  K  G  G  D  E
      GATAAAATGAAGAGAATGAATACTTTGTATAAAAAAATGGAGCAGGAT
49    D  K  M  K  R  M  N  T  L  Y  K  K  M  E  Q  D
      GTAAAGGTAGCTCATCAGCCTGATTTTGGAACCTGGAGTAGCTCAGAG
65    V  K  V  A  H  Q  P  D  F  G  T  W  S  S  S  E
      GTGCCAACCTATGGAACAGAAGAGTGGGAGTCCTGGTGGAGTTCCTTT
81    V  P  T  Y  G  T  E  E  W  E  S  W  W  S  S  F
      AATGAAAAATGGGATGAAGATTTATTTTGCCATGAAGATATGTTTGCC
97    N  E  K  W  D  E  D  L  F  C  H  E  D  M  F  A
      AGTGATGAAGAGCAACAGCAGATTCTCAACACTCAACACCACCCAAA
113   S  D  E  E  A  T  A  D  S  Q  H  S  T  P  P  K
      AAAAAAGAAAGGTAGAAGACCCTAAAGACTTTCCCTCTGATCTACACC
129   K  K  E  R  .
```

FIG 3 HIVSGD BKPyV Tag sequence analysis revealed a premature stop codon in HIVSGD-2. (A) The depicted BKPyV DNA sequences show the Tag adenosine (A) deletion found within HIVSGD-2 but not HIVSGD-1. (B) Alignment of the Tag amino acid sequences of HIVSGD-1, HIVSGD-2, and the SV40 pRb binding domain (1GH6 chain A) via ClustalW localized the deletion distal to the pRb binding domain. The deletion was predicted to alter the original PKKKRKV nuclear translocation signal found within HIVSGD-1 into PKKKER (see the box) in HIVSGD-2. (C) The deletion was further predicted to introduce an early stop codon (see the box) and subsequently truncate HIVSGD-2 Tag. Schematic models of full-length HIVSGD-1 Tag (wild type [wt], 80.5-kDa protein) and truncated HIVSGD-2 Tag (15.6-kDa protein) were created using the HHPred and MODELLER structural prediction servers (sequence and model coloring coincide). On the left is depicted the full-length sequence, and on the right are depicted the truncated sequence and schematic models, respectively.

banding patterns are detected upon comparison to DpnI digestion for both HIVSGD-1 and MM BKPyV DNA. The detection of HIVSGD-1 (Fig. 5B, lane 5 versus lane 6) and MM (Fig. 5A, lane 7 versus lane 8) DNA bands post-Sau3a digestion but not post-DpnI digestion, in the range of 100 to 1,600 bp suggested that the detected BKPyV DNA was of eukaryotic origin, and therefore HIVSGD-1 and MM BKPyV underwent whole-genome replication in HSG cells. While not all bands are distinct, they corresponded to mapped MM BKPyV (GenBank accession no. V01109.1) DpnI/Sau3a cut sites resulting in fragments ranging from 1 to 1.6 kb. BKPyV DNA bands between 1.6 and 5 kb are likely due to incomplete digestion, and prominent bands at ~5 kb

(Fig. 5A, lane 7) correspond to whole-genome BKPyV, as previously reported (9). In summary, the enzyme resistance assay suggested that both HIVSGD-1 and MM BKPyV DNA were made *de novo* in transfected HSG cells. The intention of this assay was not to compare BKPyV replication levels but to firmly establish that HIVSGD-1 BKPyV could replicate its DNA in human salivary gland cells. Faint kidney-derived U1 BKPyV DNA bands were visualized upon long exposure, suggesting potential replication (Fig. 5A, lanes 3 and 4).

Tag protein expression reflects successful transition through the early BKPyV life cycle. The consequence of the HIVSGD-2 Tag mutation on its protein expression was assessed. Levels of Tag
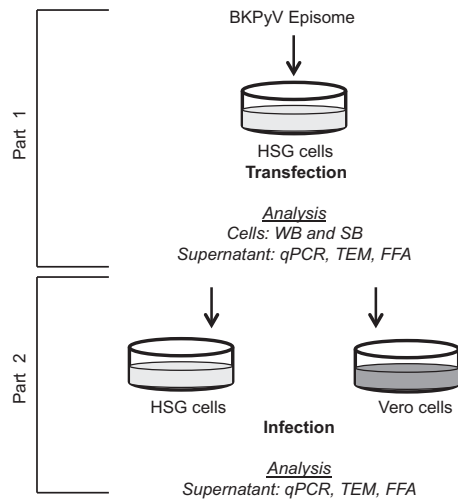
FIG 4 Multistep salivary gland cell *in vitro* system for viral fitness assessment. The diagram shows the two parts of the *in vitro* model. Part 1 represents human salivary gland cell (HSG) transfection with episomal BKPyV, and part 2 represents HSG and Vero cell infection with transfection-derived BKPyV. The following analyses were performed: Western blotting (WB) for Tag protein expression, Southern blotting (SB) for *de novo* BKPyV DNA expression, quantitative real-time PCR (qPCR) for viral load (VL) determination, fluorescent focus assay (FFA) for infectious virus quantification, and transmission electron microscopy (TEM) for virion morphology characterization.

protein expression were determined 5 days post-HSG transfection and compared among clinical isolates HIVSGD-1, HIVSGD-2, and U1 and laboratory strain MM BKPyV by Western blotting (Fig. 6A). The laboratory strain Dunlop BKPyV was not further assessed as HSG cells were unable to support DNA replication (Fig. 5). The harvest time point was selected based on previous studies that detected Tag protein expression 4 days p.t. (26, 34). Tag was normalized to expression of β-actin, a loading control (Fig. 6B). The highest Tag expression was detected for HIVSGD-1 (full-length, ~80 kDa), followed by MM and U1 BKPyV (Fig. 6B). Both full-length and truncated (~15 kDa [not shown]) forms of Tag protein were below the level of immunoblot detection for HIVSGD-2. No Tag protein was detected in mock-infected negative controls.

To further evaluate the replication potential of each isolate, encapsulated BKPyV virions released from transfected HSG cells were quantified. At 6 days p.t., BKPyV viral loads (VLs) of filtered and DNase-treated media from transfected HSG cells were determined by quantitative real-time PCR (qPCR). The supernatant of all BKPyV-transfected HSG cells carried encapsulated BKPyV DNA. MM- and HIVSGD-1-transfected HSG cells supported similarly high VLs, with 3.5×10^7 and 2.4×10^7 copies/μl, respectively. U1 and HIVSGD-2 VLs were significantly lower than that of HIVSGD-1, at 1.4×10^3 and 2.6×10^2 copies/μl, respectively (Fig. 7A). Differences between HIVSGD-2 and U1 VLs each compared to HIVSGD-1 were highly statistically significant ($P = 0.0001$). HIVSGD-1 was the most efficient replicator, followed by MM, U1, and HIVSGD-2. Interestingly, low levels of HIVSGD-2 virions were detected, despite the Tag mutation and lack of Tag expression, as described above. To confirm the presence of BKPyV virions, HSG supernatant (6 days p.t.) was analyzed by transmission electron microscopy (TEM). BKPyV particles were detected by TEM for HIVSGD-1 and MM but were not detected for lower
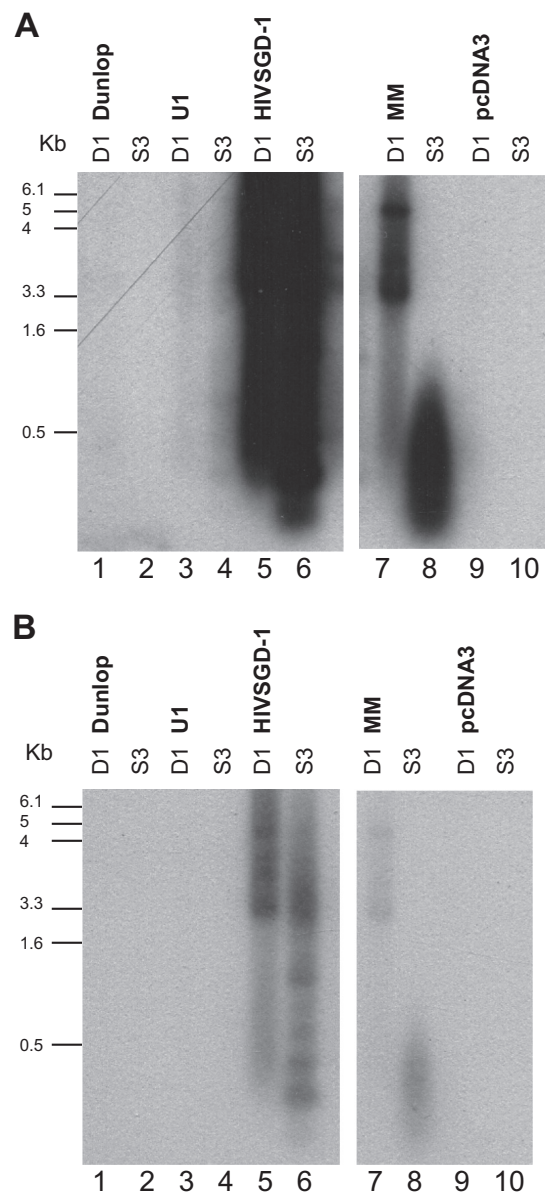
FIG 5 HIVSGD-1 and MM BKPyV DNA were made *de novo* in human salivary gland cells. Panels A and B show the same blot at different exposures (A, 15 min and B, 1 min). Low-molecular-weight DNA was isolated 6 days post-HSG cell transfection with Dunlop, MM, U1, and HIVSGD-1 BKPyV DNA. pcDNA3 DNA transfection served as the negative control. Isolated DNA was digested with endonucleases DpnI (D1) and Sau3a (S3) and visualized via Southern blotting. DpnI and Sau3a cut the same sites, but DpnI recognizes exclusively bacterial and not eukaryotic methylation patterns. DpnI resistance assay allows differentiation of BKPyV DNA that was transfected (of bacterial origin) and BKPyV DNA that was made *de novo* by HSG cells (of eukaryotic origin). Detection of stronger DNA bands (at expected size) post-Sau3a digestion versus post-DpnI digestion, as seen for BKPyV HIVSGD-1 and MM DNA (lane 5 versus lane 6 and lane 7 versus lane 8), suggested that BKPyV DNA was made *de novo* by transfected HSG cells. No Dunlop BKPyV DNA (lanes 1 and 2) and faint U1 (lanes 3 and 4) bands were found.

replicators U1 or HIVSGD-2 BKPyV (Fig. 7B). Morphological features of HIVSGD-1 and MM BKPyV were reminiscent of icosahedral (T = 7) symmetrical BKPyV particles with a diameter of 45 nm (4) that have been visualized in *in vitro*-derived supernatants (34) and patient-derived fluids (50).
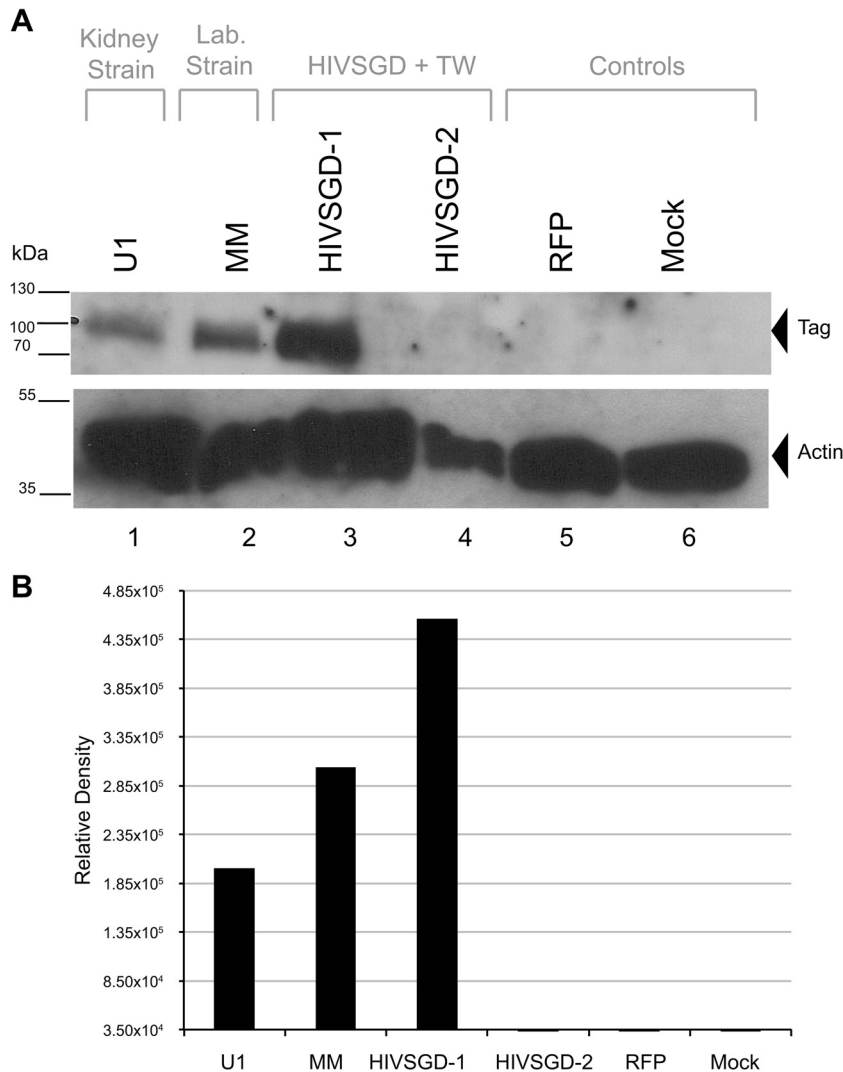
FIG 6 HIVSGD-1 but not HIVSGD-2 expressed BKPyV Tag protein post-HSG cell transfection. (A) Protein bands visualized via Western Blotting (WB). Total cell lysates were harvested 5 days p.t., and proteins were analyzed by WB, probing for viral Tag (~82 kDa) and cellular β-actin (~45 kDa; loading control). The Tag expression levels ranked from high to low as HIVSGD-1, MM, and U1 BKPyV. No HIVSGD-2 Tag protein was detected. (B) The chart shows the relative protein band density, measured by densitometry and normalized to actin.

The titer of infectious HSG transfection-derived BKPyV virions was determined via the fluorescent focus assay (FFA). FFA provided antibody-based detection of intracellular PyV proteins postinfection (44). Vero cells were exposed to HSG cell supernatant containing BKPyV and incubated for 4 days, and infected cells were quantified. Intracellular PyV structural proteins (VP1, VP2, and VP3 [green]) were detected for HIVSGD-1, HIVSGD-2, and laboratory strain MM but not for U1 BKPyV or mock infection (Fig. 8). As in previous studies (44), PyV proteins were detected exclusively in the nucleus (DAPI [blue]) of infected Vero cells (Fig. 8C). Infectious BKPyV VR837, which has been shown to replicate permissively in HSG and Vero cells (26) served as a positive control. HIVSGD-1, MM, and HIVSGD-2 scored 80, 50, and 1 FFU/µl, respectively. HIVSGD-1 infected significantly more cells than laboratory strain MM ($P = 0.01$) and HIVSGD-2 ($P = 0.0001$) (Fig. 8B). Despite detectable U1 VLs by qPCR, U1 BKPyV intracellular proteins were not detected by FFA.

Clinical and laboratory strain BKPyV postinfection. Infections were performed to assess cell-type-dependent reproduction of HSG-derived BKPyV (Fig. 4, part 2). HSG and Vero cells were simultaneously infected with equal amounts of BKPyV that originated from HSG cell transfections—an equivalent of 200 FFU for each viral substrain (Fig. 4, part 1). Encapsulated BKPyV virions released from infected HSG and Vero cells were quantified by qPCR at 2, 4, 6, and 8 days postinfection (p.i.). HIVSGD-1 and MM BKPyV VLs increased by 4 and 3 orders of magnitude, respectively, in HSG cells over 8 days p.i. In Vero cells, HIVSGD-1 and MM BKPyV VLs increased by 5 and 4 orders of magnitude, respectively, over 8 days p.i. (Fig. 9A). These results indicated that HSG cell transfection-derived HIVSGD-1 and MM BKPyV were infectious and underwent replication in both HSG and Vero cells. Encapsulated HIVSGD-2 and U1 BKPyV DNAs were not detected from either cell type. Interestingly, the VL kinetics of BKPyV in Vero and HSG cells were similar upon infection, suggesting that virion production was equally efficient in both HSG and Vero cells
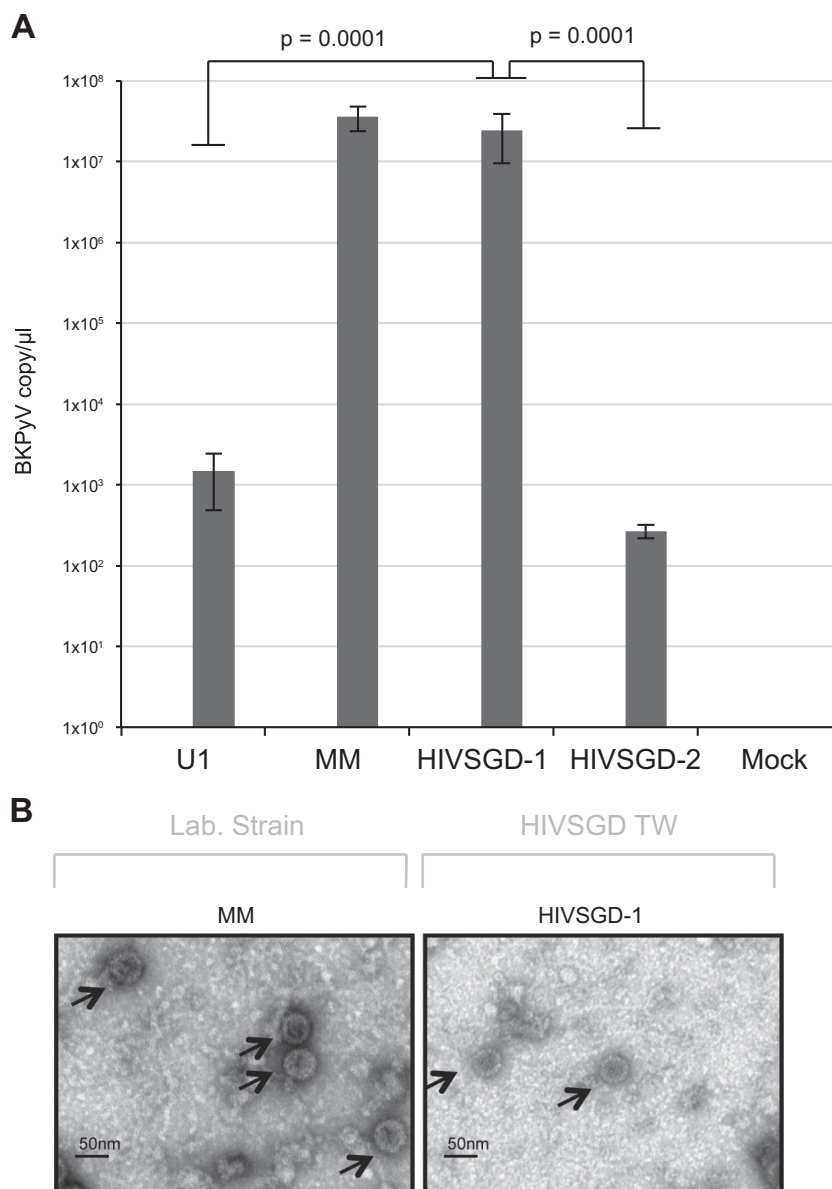
FIG 7 Significantly higher viral loads were detected for HIVSGD-1 than for HIVSGD-2 BKPyV post-HSG cell transfection. (A) The chart shows viral loads (VLs) measured from the supernatant of HSG cells transfected with BKPyV genomes. HSG cell supernatant was harvested 6 days p.t., filtered, and DNase treated, and BKPyV was quantified via qPCR and is depicted as BKPyV copies/μl. VL levels are ranked from high to low as MM, HIVSGD-1, U1, and HIVSGD-2 BKPyV. The *P* values were determined via one-way analysis of variance (ANOVA), and error bars represent standard deviations. (B) Representative images visualizing HIVSGD-1 and MM BKPyV virions from HSG cell supernatant via transmission electron microscopy (TEM) 6 days p.t. (black arrows).

postinfection. TEM confirmed BKPyV virion presence and morphology (8 days p.i.). Visualized particles were classified as BKPyV based on capsid morphology and diameter. BKPyV particles were detected in the media of HSG cells infected with HIVSGD-1 and in Vero cells infected with HIVSGD-1 and MM BKPyV (Fig. 9B). U1 and HIVSGD-2 virions were not identified upon inspection. MM BKPyV-infected HSG cell medium was not analyzed by TEM.

The infectivity of HSG- and Vero cell-derived BKPyV progeny was assessed by FFA (Fig. 10). Vero cells were infected with HSG and Vero cell media 8 days p.i. and incubated over 4 days. PyV structural proteins (VP1, VP2, and VP3 [green]) were detected at 289 FFU/μl for VR837 (positive control), and no viral proteins were detected in mock infections (Fig. 10A). HSG cell infection-

derived MM and HIVSGD-1 BKPyV both scored 48 FFU/μl, whereas U1 scored 5 FFU/μl (9.6-fold less). No infectious HIVSGD-2 BKPyV was detected (Fig. 10B). Interestingly, much lower FFUs were detected in Vero cell infection-derived MM and HIVSGD-1 BKPyV (10 FFU/μl and 19 FFU/μl, respectively) than in these viruses of HSG cell origin (48 FFU/μl). These results indicated that HIVSGD-1 and MM BKPyV were more infectious if originating from HSG (salivary gland) cells than Vero (kidney) cells (Fig. 10C and D), despite the detection of similar VLs in both cell types (Fig. 9). Most strikingly, among Vero cell-derived BKPyV, the kidney-derived virus U1 (58 FFU/μl) was most infectious and displayed 5.8-fold-higher FFU/μl than MM and 3-fold-higher FFU/μl than HIVSGD-1 BKPyV. Despite the lack of de-

A
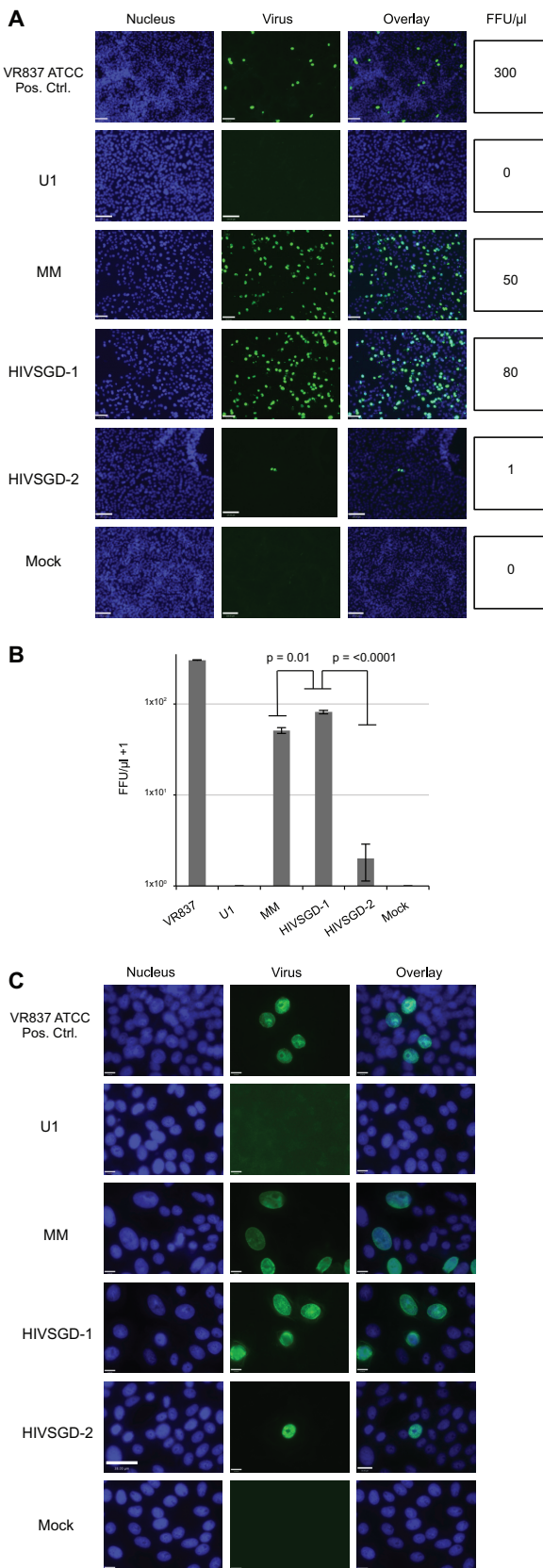
tectable VLs (Fig. 9), U1 (kidney-derived) BKPyV scored higher FFU originating from kidney (Vero) cells than salivary gland (HSG) cells (Fig. 10C and D). As expected, the lack of measurable HIVSGD-2 BKPyV VL was associated with an inability to detect infected cells, whether Vero or HSG cell derived.

DISCUSSION

HIV-associated salivary gland disease (HIVSGD) is among the most significant HIV/AIDS-associated oral lesions (25). Previously published data by our group suggested a correlation between HIVSGD and BKPyV (25, 26). To our knowledge, we are the first to analyze HIVSGD BKPyV and to establish a fully permissive salivary gland cell culture model supporting productive replication of clinical BKPyV isolates. The present study assessed replication differences in genomically similar HIVSGD isolates and compared a kidney-derived clinical isolate to HIVSGD clinical isolates. We assessed the noncoding control region (NCCR) of these isolates and determined *in vitro* replication capabilities in both salivary gland and kidney cells. Importantly, this study provides evidence for differences in cell tropism based on the cell origin of BKPyV.

Three clinical BKPyV isolates were characterized and compared: HIVSGD-1 and HIVSGD-2 were isolated from the throat wash (TW) samples of HIVSGD-positive patients, and U1 was isolated from the urine sample of an HIVSGD-negative transplant patient (kidney-associated isolate). BKPyV viral loads (VLs) from all three clinical samples were high and ranged from 1.7×10^5 to 1.7×10^9 copies/ml, likely reflecting immunosuppression in each instance. We previously established that VLs in healthy individuals and in HIV-positive patients without HIVSGD were 3 to 4 logs lower than the VLs detected in HIVSGD-positive individuals (25). Comparable VLs in the HIVSGD-associated oral fluid samples and in the urine sample from a transplant patient diagnosed with BKN suggested a significant increase in shed virus, perhaps at pathogenic levels.

Whole-genome sequence alignment of the two HIVSGD clones (HIVSGD-1 and HIVSGD-2) determined 99.9% similarity, despite three point mutations (Fig. 1A). A thymidine deletion was detected between the open reading frames (ORFs) that encoded agnoprotein and VP2 (Fig. 1A, bar 1). The deletion was outside the respective ORFs and was therefore unlikely to affect replication. Nevertheless, it was possible that the mutation could have interfered with VP2 gene expression via disruption of a potential internal ribosome entry site (IRES) that was present in this region of the BKV genome. However, the affected nucleotide stretch did not contain a known IRES (Fig. 1B).

The BKPyV NCCR is the main determinant of *in vitro* replication (9), and rearrangements confer significant differences in rep-

B

C

FIG 8 Infectious HIVSGD-1, HIVSGD-2, and MM BKPyV progeny were detected post-HSG cell transfection. (A) Representative images showing HIVSGD-1-, HIVSGD-2-, MM-, and VR837 BKPyV-infected Vero cells. Transfected HSG cell supernatant was transferred onto Vero cells, and BKPyV-infected cells were visualized via FFA. BKPyV protein (green) was detected in the nucleus (DAPI [blue]). VR837 infection served as the positive control (Pos. Ctrl.). The number of infected cells was counted for each treatment in a minimum of 10 fields at ×20 magnification, and FFU/µl values were calculated. (B) FFU values were graphed for each treatment and are depicted as FFU/µl + 1. The error bars represent standard deviations, and the *P* values were assessed via one-way ANOVA. (C) Representative images at higher magnification: IFA, 60×, oil immersion.
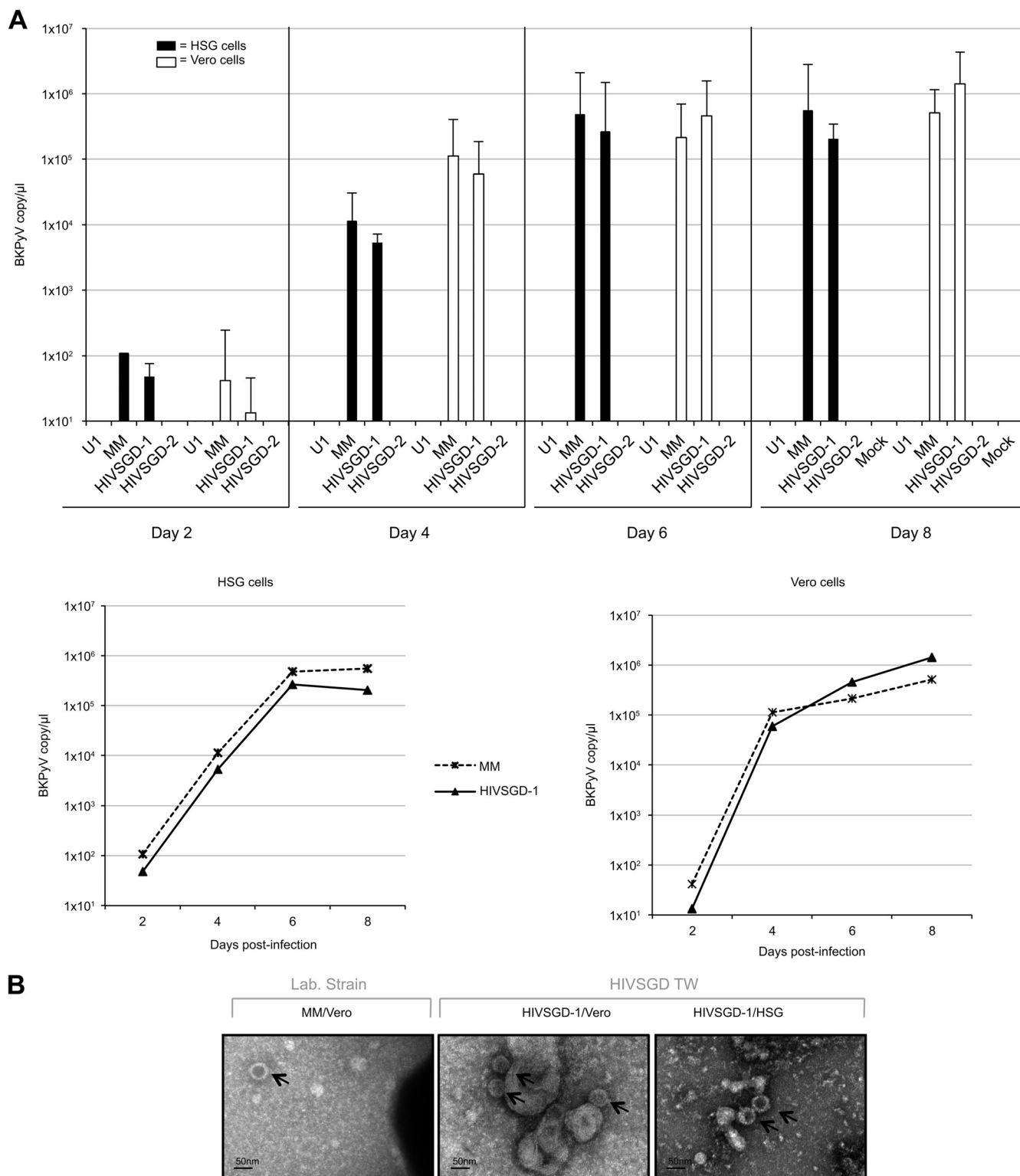
FIG 9 HIVSGD-1 and MM BKPyV exhibited similar replication kinetics in HSG and Vero cells with increasing viral loads postinfection. (A) The chart at the top shows viral loads (VLs) in BKPyV copies/µl, measured from the supernatant of infected HSG and Vero cells, 2, 4, 6, and 8 days p.i. Filtered supernatant from transfected HSG cells was used to infect HSG (black) and Vero (white) cells at equal viral loads. Supernatant from infected cells was harvested, filtered, and DNase treated, and BKPyV VL was quantified via qPCR. BKPyV HIVSGD-1 VLs increased over 6 orders of magnitude and MM VLs over 5 orders of magnitude during the 8 days p.i. Encapsulated HIVSGD-2 DNA and U1 BKPyV DNA were not detected. Error bars represent standard deviations. Graphed VLs from infected HSG cells and Vero cells show similar growth kinetics for BKPyV HIVSGD-1 and MM. (B) HIVSGD-1 (Vero- and HSG cell-derived) and MM (Vero cell-derived) BK virions were detected under TEM 8 days p.i. MM BKPyV-infected HSG supernatant was not analyzed. No virions were detected for HIVSGD-2, U1, and mock infection in HSG or Vero cells (data not shown). Mock infections were accomplished by using supernatant from mock-transfected cells.
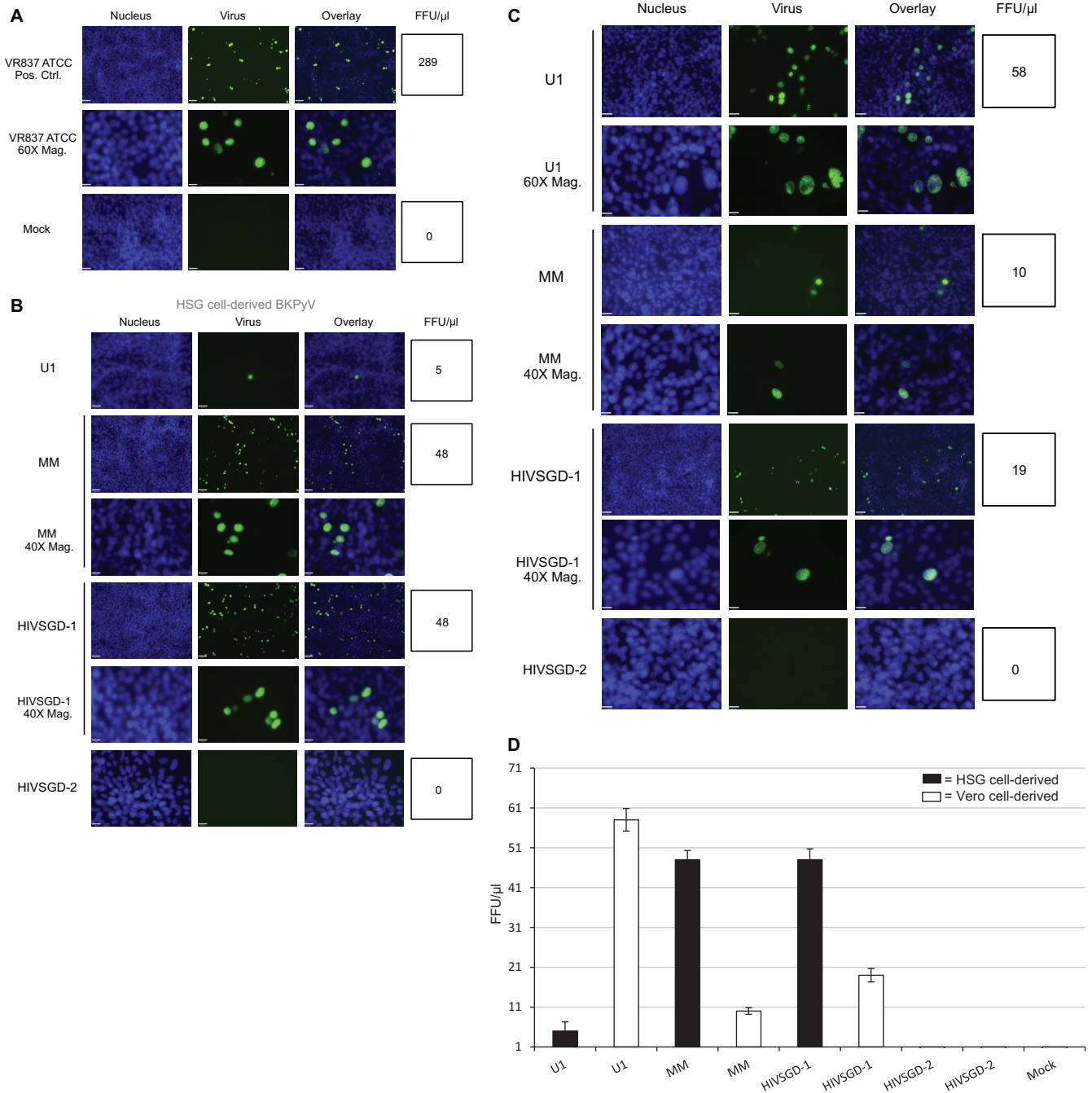
FIG 10 Cell-type-dependent differential infection was detected based on viral origin. (A) Representative images of FFA-positive (VR837 BKPyV infection; 289 FFU/μl) and FFA-negative (mock infection; no virus detected) controls. Infected cells (green) and nuclei (blue) were quantified, and FFU/μl values were calculated. A magnification (Mag.) of 60× is shown for the middle row. (B) Representative images of HIVSGD-1-, U1-, and MM BKPyV-infected cells are shown. Supernatant of infected HSG cells (8 days p.i.) was filtered and transferred onto Vero cells. HIVSGD-1 and MM yielded 48 FFU/μl. U1 yielded 5 FFU/μl. No infected cells were detected for the HIVSGD-2 treatment. (C) Representative images of HIVSGD-1-, U1-, and MM BKPyV-infected cells are shown. Supernatant of infected Vero cells (8 days p.i.) was filtered and transferred onto Vero cells. Infected cells were visualized via FFA (green) and quantified, and FFU values were calculated. HIVSGD-1 yielded 19 FFU/μl, MM yielded 10 FFU/μl, and U1 yielded 58 FFU/μl. No infected cells were detected for the HIVSGD-2 treatment. (D) The chart shows FFU values for each treatment, depicted as FFU/μl. Black bars, HSG cell infection-derived BKPyV; white bars, Vero cell infection-derived BKPyV. Error bars represent standard deviations.

lication capacity, transforming potential, host cell permissivity, and tropism (12, 37, 39, 40, 51–53). NCCR rearrangements are defined as changes in the NCCR block sequences compared to the archetype. The archetypic BKPyV substrain, defined by carrying the OPQRS NCCR architecture, is commonly shed in urine (5). We sequenced the BKPyV NCCRs of the three clinical isolates and detected a common signature block alignment, OPQPQQS, among the HIVSGD TW samples. NCCR block divergence from

archetype into rearranged (rr) variants, as detected in this study, have been previously recorded both *in vivo* (16, 51, 54, 55) and *in vitro* (16, 35, 37, 38, 56). Prior studies among transplant recipients with prolonged viremia illustrated that rearranged architectures eventually became dominant over the archetype (39). The rr NCCR OPQPQQS may reflect the dominant architecture within these HIVSGD patients and may represent a stable and biologically significant variant. Despite VP1-based classification of BKPyV genotypes (57), BKPyV variants are categorized by NCCR block sequence (58). The OPQPQQS NCCR block alignment was previously described in laboratory strain MM; however, to our knowledge, other clinical isolates carrying this architecture have not been reported. Importantly, underlying nucleotide differences distinguished the HIVSGD clinical isolates from MM. Inclusion of well-described BKPyV laboratory strains during NCCR genotyping corroborated the authenticity of our results.

HIVSGD-1 and MM BKPyV shared the NCCR OPQPQQS block architecture and exhibited similar levels of Tag expression, virion production, and infectivity. Similar replication efficiency between HIVSGD-1 and MM may be explained by the analogous NCCR architecture. HIVSGD-2, however, consistently lacked signs of efficient *in vitro* replication. While HIVSGD-2 shared the overall NCCR architecture with HIVSGD-1 and MM, the HIVSGD-2 NCCR S block contained a thymidine (T)/cytidine (C) transition (Fig. 1A, no. 2). This NCCR transition did not lead to differential prediction of putative human TFBS (Fig. 2A) or to differences in the early promoter activity in the presence or absence of full-length Tag (Fig. 2B) and thus was an unlikely contributor to differences in replication efficiency. Interestingly, the HIVSGD-2 promoter in the late direction was induced more readily, in the presence or absence of full-length Tag, than the high replicator HIVSGD-1 (Fig. 2C). Based on *in vitro* results that characterized HIVSGD-2 as an inefficient replicator, higher HIVSGD-2 promoter activity in the late direction was unlikely to affect its viral fitness. Despite the well-documented importance of the NCCR for BKPyV replication, the S block point mutation appeared unlikely to affect viral fitness.

Inefficient HIVSGD-2 replication was likely associated with the adenosine deletion distal to the Tag pRb binding domain. This point mutation was predicted to introduce an early stop codon and modify the nuclear translocation signal (Fig. 3A and B). This resulted in the expression of a truncated form of Tag that decreased the predicted Tag protein size from 80.5 kDa to 15.6 kDa. The mutant form of Tag lost the origin-binding domain (OBD), p53 site, and ATP/helicase domain (Fig. 3C) and carried a modified version of the nuclear translocation signal (Fig. 3A and B). Tag is central to genome replication and PyV life cycle completion (59–61). Insufficient Tag expression has been shown to impede archetypic BKPyV replication *in vitro* (34). It is therefore likely that insufficient Tag expression dramatically inhibited HIVSGD-2 replication. Remarkably, the isolation of HIVSGD-2 BKPyV from the TW sample and generation of progeny virus served as evidence of minimal HIVSGD-2 replication both *in vivo* and *in vitro*. HIVSGD-2 virus was detected at low levels posttransfection, as determined by qPCR (VL measurement in Fig. 7), and was infectious, as measured by FFA (Fig. 8). Two potential mechanisms may have allowed for low levels of HIVSGD-2 replication. (i) *In vivo*, the first mechanism is provision of Tag in *trans* by other BKPyV substrains. Broekema et al. demonstrated that provision of overexpressed Tag allowed the cultivation of archetype BKPyV,

a typically low *in vitro* replicator (34). (ii) *In vitro* and *in vivo*, by the second mechanism, low levels of full-length Tag could be produced by ribosomal frameshifting. Ribosomal frameshifting commonly takes place in retroviruses facilitated by a slippery A/T-rich heptanucleotide sequence that allows for low protein expression despite the presence of a stop codon (62). The A/T-rich stretch within HIVSGD-2 BKPyV Tag located 5′ to the stop codon may allow for frameshifting in the context of BKPyV. Moreover, premature truncations of Tag have been detected in other PyVs. Merkel cell polyomavirus (MCV) mutations that prematurely truncated Tag were found in strains derived from human tumors but not in benign sources and have been postulated to render MCV more malignant (60). Likewise, there is the potential that truncation of HIVSGD BKPyV Tag not only may decrease replication efficiency but also may be associated with increased *in vivo* transformation potential.

HIVSGD BKPyV *in vitro* viability was assessed by transfection (Fig. 4, part 1) and infection (Fig. 4, part 2) of salivary gland cells and kidney cells. Kidney cells represented the historically described replication niche. HIVSGD BKPyV fitness was compared to those of both kidney-derived substrain U1 and laboratory strain MM (Table 1). We hypothesized that shed HIVSGD isolates were likely to replicate in salivary gland cells *in vivo*, and by extension, these isolates would replicate efficiently within HSG cells *in vitro*. Indeed, HIVSGD-1 consistently exhibited high replication competence in salivary gland cells. HIVSGD-1 and MM demonstrated the highest posttransfection replication efficiency compared to HIVSGD-2 and kidney-derived U1, as determined by viral protein concentrations (Fig. 6), VLs (Fig. 7), and significant levels of infectious BKPyV progeny (Fig. 8). Furthermore, the high replication capability of HIVSGD-1 was consistent during infection of HSG and Vero cells (Fig. 4, part 2) with high levels of HSG cell-released progeny virus (Fig. 9). HIVSGD-1, MM, and U1 but not HIVSGD-2 completed a full life cycle upon secondary viral passage.

HIVSGD-1 and MM VL measurements suggested equally efficient levels of virion production upon infection of HSG and Vero cells, as the replication kinetics were very similar (Fig. 9). Differences in scored infectious units, however, suggested that while replication kinetics and progeny output were consistent for HIVSGD-1 and MM, subsequent infectivity was distinct, depending on cell type and virus origin comparing HIVSGD-1 or MM versus kidney-derived U1 (Fig. 10D). When HIVSGD-1 and MM BKPyV originated from HSG cells rather than Vero cells higher FFU were scored. Likewise, when kidney-derived U1 BKPyV originated from Vero cells rather than HSG cells, higher FFU were scored. Differential infectivity suggested HIVSGD BKPyV displayed preferential tropism for salivary gland cells over kidney cells. Similarly, U1 displayed preferential tropism for kidney cells over salivary gland cells. Additionally, we recorded a dramatic increase in viral progeny production for Vero cell-derived U1 during the 4-day Vero cell incubation for the FFA (Fig. 10). This was interesting since U1 VLs were below the level of detection for qPCR quantification at 8 days p.i. (Fig. 9) and suggested that kidney-derived U1 BKPyV was able to produce infectious progeny more efficiently in kidney cells (58 FFU/μl) than HSG cells (5 FFU/μl) (Fig. 10). Overall, differential infectivity depending on cell origin suggested that U1 displayed kidney tropism and HIVSGD BKPyV displayed salivary gland tropism, consistent with their respective *in vivo* kidney and salivary gland origins. Interest-

ingly, previous studies comparing levels of laboratory strain BKPyV replication among a wide range of different cell lines detected few differences in replication potential and did not indicate specific cellular tropisms (63, 64). These studies assessed over 60 cell types: among them were lung-, colon-, central nervous system (CNS)-, ovary-, renal-, and bladder-derived cell lines. Salivary gland cells were not assessed.

BKPyV isolated from the TW of HIVSGD patients is likely relevant to disease in the *in vivo* setting and has now undergone initial *in vitro* characterization. High BKPyV VLs were detected in the oral fluids of two individuals diagnosed with HIVSGD. We identified a common NCCR block architecture among HIVSGD-derived BKPyV isolates and successfully cultured clinical HIVSGD-derived BKPyV in human salivary gland cells and in kidney cells. Our assessment of a high-replication clinical isolate and a low-replication clinical isolate suggested that a single point mutation in Tag brought about the stark differences in the *in vitro* replication potential. The high replicator (HIVSGD-1) surpassed the replication potential of the kidney-derived isolate (U1) in human salivary gland cells, replicated efficiently in human salivary gland and kidney cells, and displayed signs of salivary gland tropism.

Our results are significant, as they corroborate a potential connection between BKPyV and HIVSGD and provide an important initial understanding of BKV replication in the oral compartment. Our data suggest that HIVSGD TW-derived BKPyV displays preferential tropism for salivary gland cells, and we have now proven that wild-type oral-clinical BKV isolates undergo permissive replication in salivary gland cells *in vitro*. Permissive replication of wild-type clinical BKV isolates previously thought to occur predominantly in renal epithelium and uro-epithelium may be ongoing at other sites as well. Saliva serves as a transmission vehicle for many microorganisms, and our data corroborate previous data showing that the oral compartment and saliva may function as a transmission vehicle for BKPyV *in vivo* as well. The small number of characterized HIVSGD isolates is a clear limitation of this current study and thus may not be representative of all HIVSGD variants. A study encompassing a larger number of isolates would be more representative and needs to be performed. Importantly, this study provides a system for the study of clinical oral BKPyV infection, and these observations provide insights for future BKPyV pathogenesis, transmission, and disease association studies.

ACKNOWLEDGMENTS

REFERENCES

1. **Gardner SD, Field AM, Coleman DV, Hulme B.** 1971. New human papovavirus (B.K.) isolated from urine after renal transplantation. Lancet **i:**1253–1257.
2. **Kean JM, Rao S, Wang M, Garcea RL.** 2009. Seroepidemiology of human polyomaviruses. PLoS Pathog. **5:**e1000363. http://dx.doi.org/10.1371/journal.ppat.1000363.
3. **Knowles WA.** 2006. Discovery and epidemiology of the human polyomaviruses BK virus (BKV) and JC virus (JCV). Adv. Exp. Med. Biol. **577:**19–45. http://dx.doi.org/10.1007/0-387-32957-9_2.
4. **Knipe DM, Howley PM, Griffin DE, Lamb RA, Martin MA, Roizman B, Straus SE** (ed). 2007. Fields virology, 5th ed. Lippincott Williams & Wilkins, Philadelphia, PA.
5. **Reploeg MD, Storch GA, Clifford DB.** 2001. BK virus: a clinical review. Clin. Infect. Dis. **33:**191–202. http://dx.doi.org/10.1086/321813.
6. **Egli A, Binggeli S, Bodaghi S, Dumoulin A, Funk GA, Khanna N, Leuenberger D, Gosert R, Hirsch HH.** 2007. Cytomegalovirus and polyomavirus BK posttransplant. Nephrol. Dial. Transplant. **22**(Suppl 8)**:** viii72–viii82. http://dx.doi.org/10.1093/ndt/gfm648.
7. **Nickeleit V, Mihatsch MJ.** 2006. Polyomavirus nephropathy in native kidneys and renal allografts: an update on an escalating threat. Transpl. Int. **19:**960–973. http://dx.doi.org/10.1111/j.1432-2277.2006.00360.x.
8. **Bohl DL, Brennan DC.** 2007. BK virus nephropathy and kidney transplantation. Clin. J. Am. Soc. Nephrol. **2**(Suppl 1)**:**S36–S46. http://dx.doi.org/10.2215/CJN.00920207.
9. **Broekema NM, Abend JR, Bennett SM, Butel JS, Vanchiere JA, Imperiale MJ.** 2010. A system for the analysis of BKV non-coding control regions: application to clinical isolates from an HIV/AIDS patient. Virology **407:**368–373. http://dx.doi.org/10.1016/j.virol.2010.08.032.
10. **Markowitz RB, Dynan WS.** 1988. Binding of cellular proteins to the regulatory region of BK virus DNA. J. Virol. **62:**3388–3398.
11. **Gorrill TS, Khalili K.** 2005. Cooperative interaction of p65 and C/EBP-beta modulates transcription of BKV early promoter. Virology **335:**1–9. http://dx.doi.org/10.1016/j.virol.2005.02.006.
12. **Johnsen JI, Seternes OM, Johansen T, Moens U, Mantyjarvi R, Traavik T.** 1995. Subpopulations of non-coding control region variants within a cell culture-passaged stock of BK virus: sequence comparisons and biological characteristics. J. Gen. Virol. **76:**1571–1581.
13. **Cho S, Tian Y, Benjamin TL.** 2001. Binding of p300/CBP co-activators by polyoma large T antigen. J. Biol. Chem. **276:**33533–33539. http://dx.doi.org/10.1074/jbc.M102906200.
14. **Abend JR, Joseph AE, Das D, Campbell-Cecen DB, Imperiale MJ.** 2009. A truncated T antigen expressed from an alternatively spliced BK virus early mRNA. J. Gen. Virol. **90:**1238–1245. http://dx.doi.org/10.1099/vir.0.009159-0.
15. **Tognon M, Corallini A, Martini F, Negrini M, Barbanti-Brodano G.** 2003. Oncogenic transformation by BK virus and association with human tumors. Oncogene **22:**5192–5200. http://dx.doi.org/10.1038/sj.onc.1206550.
16. **Bennett SM, Broekema NM, Imperiale MJ.** 2012. BK polyomavirus: emerging pathogen. Microbes Infect. **14:**672–683. http://dx.doi.org/10.1016/j.micinf.2012.02.002.
17. **White MK, Safak M, Khalili K.** 2009. Regulation of gene expression in primate polyomaviruses. J. Virol. **83:**10846–10856. http://dx.doi.org/10.1128/JVI.00542-09.
18. **Khalili K, Stoner GL.** 2001. Human polyomaviruses: molecular and clinical perspectives. Wiley, New York, NY.
19. **Pearson Education, Inc.** 2008. Number of U.S. transplants per year, 1988–2008. Pearson Education. Inc. www.infoplease.com/science/health/us-transplants-year-1988-2007.html.
20. **Vanchiere JA, Abudayyeh S, Copeland CM, Lu LB, Graham DY, Butel JS.** 2009. Polyomavirus shedding in the stool of healthy adults. J. Clin. Microbiol. **47:**2388–2391. http://dx.doi.org/10.1128/JCM.02472-08.
21. **Comar M, Zanotta N, Bovenzi M, Campello C.** 2010. JCV/BKV and SV40 viral load in lymphoid tissues of young immunocompetent children from an area of north-east Italy. J. Med. Virol. **82:**1236–1240. http://dx.doi.org/10.1002/jmv.21786.
22. **Comar M, Zanotta N, Rossi T, Pelos G, D'Agaro P.** 2011. Secondary lymphoid tissue as an important site for WU polyomavirus infection in immunocompetent children. J. Med. Virol. **83:**1446–1450. http://dx.doi.org/10.1002/jmv.22124.
23. **Babakir-Mina M, Ciccozzi M, Trento E, Perno CF, Ciotti M.** 2009. KI and WU polyomaviruses in patients infected with HIV-1, Italy. Emerg. Infect. Dis. **15:**1323–1325. http://dx.doi.org/10.3201/eid1508.090424.
24. **Bialasiewicz S, Whiley DM, Lambert SB, Nissen MD, Sloots TP.** 2009. Detection of BK, JC, WU, or KI polyomaviruses in faecal, urine, blood, cerebrospinal fluid and respiratory samples. J. Clin. Virol. **45:**249–254. http://dx.doi.org/10.1016/j.jcv.2009.05.002.
25. **Jeffers L, Webster-Cyriaque JY.** 2011. Viruses and salivary gland disease (SGD): lessons from HIV SGD. Adv. Dent. Res. **23:**79–83. http://dx.doi.org/10.1177/0022034510396882.

26. **Jeffers LK, Madden V, Webster-Cyriaque J.** 2009. BK virus has tropism for human salivary gland cells in vitro: implications for transmission. Virology **394:**183–193. http://dx.doi.org/10.1016/j.virol.2009.07.022.

27. **Shanti RM, Aziz SR.** 2009. HIV-associated salivary gland disease. Oral Maxillofac. Surg. Clin. North Am. **21:**339–343. http://dx.doi.org/10.1016/j.coms.2009.04.002.

28. **Terry JH, Loree TR, Thomas MD, Marti JR.** 1991. Major salivary gland lymphoepithelial lesions and the acquired immunodeficiency syndrome. Am. J. Surg. **162:**324–329. http://dx.doi.org/10.1016/0002-9610(91)90141-Y.

29. **DiGiuseppe JA, Corio RL, Westra WH.** 1996. Lymphoid infiltrates of the salivary glands: pathology, biology and clinical significance. Curr. Opin. Oncol. **8:**232–237. http://dx.doi.org/10.1097/00001622-199605000-00011.

30. **Ioachim HL, Ryan JR.** 1988. Salivary gland lymphadenopathies associated with AIDS. Hum. Pathol. **19:**616–617. http://dx.doi.org/10.1016/S0046-8177(88)80220-X.

31. **Schiodt M, Dodd CL, Greenspan D, Daniels TE, Chernoff D, Hollander H, Wara D, Greenspan JS.** 1992. Natural history of HIV-associated salivary gland disease. Oral Surg. Oral Med. Oral Pathol. **74:**326–331. http://dx.doi.org/10.1016/0030-4220(92)90069-3.

32. **Islam NM, Bhattacharyya I, Cohen DM.** 2012. Salivary gland pathology in HIV patients. Diagn. Histopathol. **18:**366–372. http://dx.doi.org/10.1016/j.mpdhp.2012.08.001.

33. **Gollard RP, Slavkin HC, Snead ML.** 1992. Polyoma virus-induced murine odontogenic tumors. Oral Surg. Oral Med. Oral Pathol. **74:**761–767. http://dx.doi.org/10.1016/0030-4220(92)90405-F.

34. **Broekema NM, Imperiale MJ.** 2012. Efficient propagation of archetype BK and JC polyomaviruses. Virology **422:**235–241. http://dx.doi.org/10.1016/j.virol.2011.10.026.

35. **Rubinstein R, Schoonakker BC, Harley EH.** 1991. Recurring theme of changes in the transcriptional control region of BK virus during adaptation to cell culture. J. Virol. **65:**1600–1604.

36. **Olsen GH, Hirsch HH, Rinaldo CH.** 2009. Functional analysis of polyomavirus BK non-coding control region quasispecies from kidney transplant recipients. J. Med. Virol. **81:**1959–1967. http://dx.doi.org/10.1002/jmv.21605.

37. **Sundsfjord A, Johansen T, Flaegstad T, Moens U, Villand P, Subramani S, Traavik T.** 1990. At least two types of control regions can be found among naturally occurring BK virus strains. J. Virol. **64:**3864–3871.

38. **Hanssen Rinaldo C, Hansen H, Traavik T.** 2005. Human endothelial cells allow passage of an archetypal BK virus (BKV) strain—a tool for cultivation and functional studies of natural BKV strains. Arch. Virol. **150:**1449–1458. http://dx.doi.org/10.1007/s00705-005-0511-3.

39. **Gosert R, Rinaldo CH, Funk GA, Egli A, Ramos E, Drachenberg CB, Hirsch HH.** 2008. Polyomavirus BK with rearranged noncoding control region emerge in vivo in renal transplant patients and increase viral replication and cytopathology. J. Exp. Med. **205:**841–852. http://dx.doi.org/10.1084/jem.20072097.

40. **Funk GA, Gosert R, Hirsch HH.** 2007. Viral dynamics in transplant patients: implications for disease. Lancet Infect. Dis. **7:**460–472. http://dx.doi.org/10.1016/S1473-3099(07)70159-7.

41. **Robaina TF, Mendes GS, Benati FJ, Pena GA, Silva RC, Montes MA, Janini ME, Camara FP, Santos N.** 2013. Shedding of polyomavirus in the saliva of immunocompetent individuals. J. Med. Virol. **85:**144–148. http://dx.doi.org/10.1002/jmv.23453.

42. **Yang RC, Wu R.** 1979. BK virus DNA: complete nucleotide sequence of a human tumor virus. Science **206:**456–462. http://dx.doi.org/10.1126/science.228391.

43. **Shirasuna K, Sato M, Miyazaki T.** 1981. A neoplastic epithelial duct cell line established from an irradiated human salivary gland. Cancer **48:**745–752.

44. **Moriyama T, Sorokin A.** 2009. BK virus (BKV): infection, propagation, quantitation, purification, labeling, and analysis of cell entry. Curr. Protoc. Cell Biol. Chapter 26:Unit 26.2. http://dx.doi.org/10.1002/0471143030.cb2602s42.

45. **Ziegler K, Bui T, Frisque RJ, Grandinetti A, Nerurkar VR.** 2004. A rapid in vitro polyomavirus DNA replication assay. J. Virol. Methods **122:**123–127. http://dx.doi.org/10.1016/j.jviromet.2004.08.012.

46. **Ding R, Medeiros M, Dadhania D, Muthukumar T, Kracker D, Kong JM, Epstein SR, Sharma VK, Seshan SV, Li B, Suthanthiran M.** 2002. Noninvasive diagnosis of BK virus nephritis by measurement of messenger RNA for BK virus VP1 in urine. Transplantation **74:**987–994. http://dx.doi.org/10.1097/00007890-200210150-00016.

47. **Larkin MA, Blackshields G, Brown NP, Chenna R, McGettigan PA, McWilliam H, Valentin F, Wallace IM, Wilm A, Lopez R, Thompson JD, Gibson TJ, Higgins DG.** 2007. Clustal W and Clustal X version 2.0. Bioinformatics **23:**2947–2948. http://dx.doi.org/10.1093/bioinformatics/btm404.

48. **Soding J, Biegert A, Lupas AN.** 2005. The HHpred interactive server for protein homology detection and structure prediction. Nucleic Acids Res. **33:**W244–W248. http://dx.doi.org/10.1093/nar/gki408.

49. **Pipas JM, Peden KW, Nathans D.** 1983. Mutational analysis of simian virus 40 T antigen: isolation and characterization of mutants with deletions in the T-antigen gene. Mol. Cell. Biol. **3:**203–213.

50. **Singh HK, Madden V, Shen YJ, Thompson BD, Nickeleit V.** 2006. Negative-staining electron microscopy of the urine for the detection of polyomavirus infections. Ultrastruct. Pathol. **30:**329–338. http://dx.doi.org/10.1080/01913120600932347.

51. **Olsen GH, Andresen PA, Hilmarsen HT, Bjorang O, Scott H, Midtvedt K, Rinaldo CH.** 2006. Genetic variability in BK virus regulatory regions in urine and kidney biopsies from renal-transplant patients. J. Med. Virol. **78:**384–393. http://dx.doi.org/10.1002/jmv.20551.

52. **Moens U, Van Ghelue M.** 2005. Polymorphism in the genome of non-passaged human polyomavirus BK: implications for cell tropism and the pathological role of the virus. Virology **331:**209–231. http://dx.doi.org/10.1016/j.virol.2004.10.021.

53. **Barcena-Panero A, Echevarria JE, Van Ghelue M, Fedele G, Royuela E, Gerits N, Moens U.** 2012. BK polyomavirus with archetypal and rearranged non-coding control regions is present in cerebrospinal fluids from patients with neurological complications. J. Gen. Virol. **93:**1780–1794. http://dx.doi.org/10.1099/vir.0.042143-0.

54. **Chatterjee M, Weyandt TB, Frisque RJ.** 2000. Identification of archetype and rearranged forms of BK virus in leukocytes from healthy individuals. J. Med. Virol. **60:**353–362.

55. **Perets TT, Silberstein I, Rubinov J, Sarid R, Mendelson E, Shulman LM.** 2009. High frequency and diversity of rearrangements in polyomavirus BK noncoding regulatory regions cloned from urine and plasma of Israeli renal transplant patients and evidence for a new genetic subtype. J. Clin. Microbiol. **47:**1402–1411. http://dx.doi.org/10.1128/JCM.02065-08.

56. **Sundsfjord A, Flaegstad T, Flo R, Spein AR, Pedersen M, Permin H, Julsrud J, Traavik T.** 1994. BK and JC viruses in human immunodeficiency virus type 1-infected persons: prevalence, excretion, viremia, and viral regulatory regions. J. Infect. Dis. **169:**485–490. http://dx.doi.org/10.1093/infdis/169.3.485.

57. **Luo C, Bueno M, Kant J, Martinson J, Randhawa P.** 2009. Genotyping schemes for polyomavirus BK, using gene-specific phylogenetic trees and single nucleotide polymorphism analysis. J. Virol. **83:**2285–2297. http://dx.doi.org/10.1128/JVI.02180-08.

58. **Memon IA, Parikh BA, Gaudreault-Keener M, Skelton R, Storch GA, Brennan DC.** 2012. Progression from sustained BK viruria to sustained BK viremia with immunosuppression reduction is not associated with changes in the noncoding control region of the BK virus genome. J. Transplant. **2012:**761283. http://dx.doi.org/10.1155/2012/761283.

59. **Feng H, Shuda M, Chang Y, Moore PS.** 2008. Clonal integration of a polyomavirus in human Merkel cell carcinoma. Science **319:**1096–1100. http://dx.doi.org/10.1126/science.1152586.

60. **Shuda M, Feng H, Kwun HJ, Rosen ST, Gjoerup O, Moore PS, Chang Y.** 2008. T antigen mutations are a human tumor-specific signature for Merkel cell polyomavirus. Proc. Natl. Acad. Sci. U. S. A. **105:**16272–16277. http://dx.doi.org/10.1073/pnas.0806526105.

61. **Campbell KS, Mullane KP, Aksoy IA, Stubdal H, Zalvide J, Pipas JM, Silver PA, Roberts TM, Schaffhausen BS, DeCaprio JA.** 1997. DnaJ/hsp40 chaperone domain of SV40 large T antigen promotes efficient viral DNA replication. Genes Dev. **11:**1098–1110. http://dx.doi.org/10.1101/gad.11.9.1098.

62. **Reil H, Kollmus H, Weidle UH, Hauser H.** 1993. A heptanucleotide sequence mediates ribosomal frameshifting in mammalian cells. J. Virol. **67:**5579–5584.

63. **Li R, Sharma BN, Linder S, Gutteberg TJ, Hirsch HH, Rinaldo CH.** 2013. Characteristics of polyomavirus BK (BKPyV) infection in primary human urothelial cells. Virology **440:**41–50. http://dx.doi.org/10.1016/j.virol.2013.01.024.

64. **Schowalter RM, Reinhold WC, Buck CB.** 2012. Entry tropism of BK and Merkel cell polyomaviruses in cell culture. PLoS One **7:**e42181. http://dx.doi.org/10.1371/journal.pone.0042181.